ACS APPLIED MATERIALS & INTERFACES

Research Article

www.acsami.org

Imaging Intracellular Anticancer Drug Delivery by Self-Assembly Micelles with Aggregation-Induced Emission (AIE Micelles)

Chunqiu Zhang,[§,†] Shubin Jin,[§,†] Shengliang Li,[†] Xiangdong Xue,[†] Juan Liu,[†] Yuran Huang,[†] Yonggang Jiang,[†] Wei-Qiang Chen,[‡] Guozhang Zou,*[,†] and Xing-Jie Liang*[,†]

[†]CAS Key Laboratory for Biological Effects of Nanomaterials & Nanosafety, National Center for Nanoscience and Technology, No. 11 Beiyitiao, Zhongguancun, Beijing 100190, China

[‡]Institute of Modern Physics, Chinese Academy of Sciences, Lanzhou 730000, China

Supporting Information

ABSTRACT: Nanoformulations show many therapeutic advantages over conventional formulations. We seek to develop traceable nanoformulations in order to closely monitor delivery. Herein, we developed a new drug delivery system (DDS) using tetraphenylethene (TPE) to fabricate a self-assembly micelle with aggregation-induced emission (AIE micelle). AIE makes the nanocarriers visible for high-quality imaging, and the switching on and off of the AIE is intrinsically controlled by the assembly and disassembly of the micelles. This DDS was tested for doxorubicin (DOX) delivery and intracellular imaging. For the DOX-loaded micelles (TPED), the DOX content reached as much as 15.3% by weight, and the anticancer efficiency was higher than for free DOX. Meanwhile, high-quality imaging was obtained to trace the intracellular delivery of the TPED.

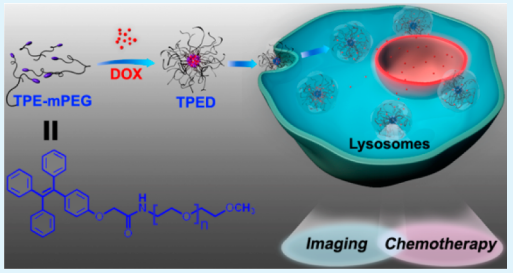

KEYWORDS: *tetraphenylethene, self-assembly micelle, aggregation-induced emission, imaging, drug delivery*

INTRODUCTION

Nanovehicles such as dendrimers,[1−4] vesicles,[5,6] liposomes,[7−13] micelles,[14−17] and inorganic materials[18−24] have been widely employed as drug delivery systems (DDSs) in cancer therapy owing to their improved pharmacokinetics and pharmacodynamics arising from the enhanced permeation and retention (EPR) effect.[25,26] Nevertheless, these traditional DDSs are typically "one trick ponies", and their sole role is to deliver drugs into cancer cells. Additionally, these DDSs are invisible and difficult to trace after they enter the cells and release the drugs. So it is desirable to develop "visible" nanovehicles to trace their distribution in cancer cells during delivery.

Recently, new-generation DDSs with the capacity for simultaneous imaging and therapeutic treatment have received more and more attention.[27−30] To make the vehicle visible, fluorescent dyes can be linked to or encapsulated in DDSs.[31,32] We instead turned to molecules with aggregation-induced emission (AIE) and constructed drug carriers with "turn on" fluorescence that is activated upon assembly.[33] Previously, we prepared tetraphenylethene (TPE)−doxorubicin (DOX) nanoparticles and studied the intracellular delivery of the DOX by measuring the fluorescence resonance energy transfer (FRET) between TPE and DOX.[34] The group of Liu and Tang also took advantage of the unique "turn on" fluorescence of AIE molecules. They designed a prodrug consisting of cisplatin conjugated to TPE through an enzyme-cleavable peptide sequence, which released cisplatin and simultaneously reported the event upon being cleaved by intracellular protease.[35]

In this study, we introduced PEG, an FDA-approved polymer with good biocompatibility, into our design to improve our delivery system. We conjugated PEG with TPE and used the conjugate to prepare amphiphilic polymeric micelles with aggregation-induced emission (AIE micelles) for delivery and simultaneous imaging to trace intracellular anticancer drug delivery as illustrated in Figure 1. Amino-methoxypolyethylene glycol ($mPEG_{2000}$−NH_2) was chosen as the hydrophilic arm. The hydrophobic TPE moiety was used as the core, which played two roles here, i.e. the luminogenic agent for imaging and the hydrophobic moiety of the DDS for entrapping hydrophobic anticancer drugs. TPE is a typical AIE building block for the construction of efficient luminescent materials.[36] It shows high emission efficiency when it is aggregated in a non-benign solvent, while the fluorescence of traditional chromophores is quenched because of the aggregation-caused quenching (ACQ) effect. AIE can completely eliminate the ACQ effect; the switching on and off of AIE is actually dynamically related to the intactness of the delivery vesicle, and the intrinsic emission from the AIE moiety endows this DDS with its self-localization feature. TPE also has the merits of facile synthesis, good photo-stability (except for UV irradiation) and accessible functionalization.[37−39] On the basis of this design, we speculatively grafted $mPEG$−NH_2 to carboxylated tetraphenylethylene (TPE−COOH) and used this conjugate to

Received: January 24, 2014
Accepted: March 10, 2014
Published: March 10, 2014

   dx.doi.org/10.1021/am5005267 | ACS Appl. Mater. Interfaces 2014, 6, 5212−5220

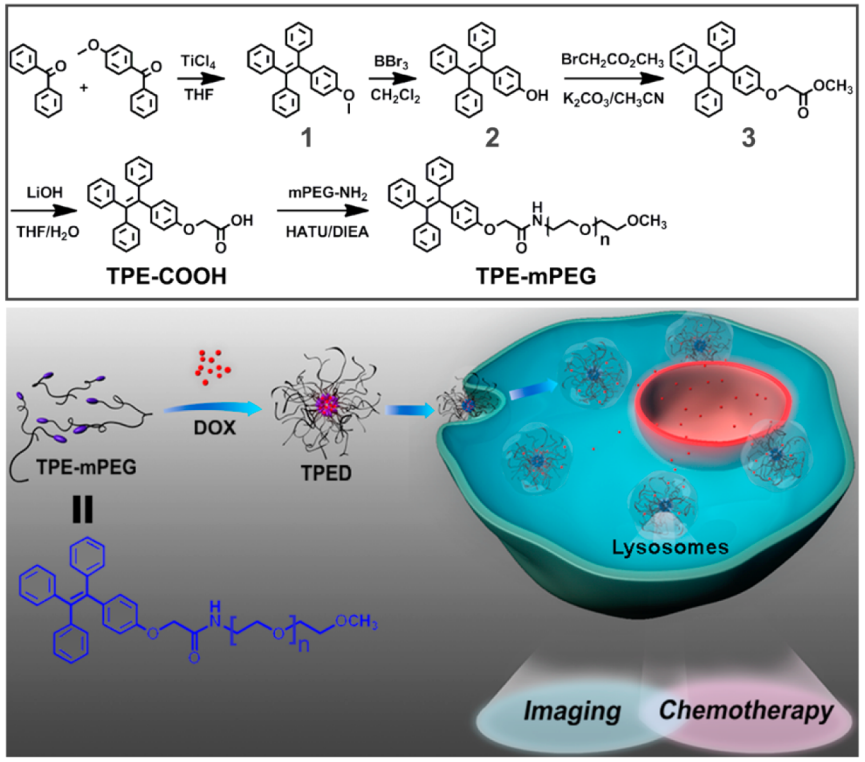

Figure 1. Synthetic route of TPE−mPEG and schematic illustration of DOX-loaded self-assembly micelle (TPED) with aggregation-induced emission (AIE) as a novel multifunctional theranostic platform for intracellular imaging and cancer treatment.

create a unique self-assembling AIE micelle for intracellular tracing of anticancer drug delivery. Its imaging quality, high drug-loading content, cellular uptake, cytotoxicity, and anticancer efficiency in vitro were investigated in detail.

RESULTS AND DISCUSSION

Preparation and Characterization of AIE Micelles. The synthesis scheme of TPE−mPEG is shown in Figure 1. The synthesized TPE−COOH was characterized by electrospray ionization mass spectroscopy (ESI-MS) and high-performance liquid chromatogrphy (HPLC; Figure 2A and B). The structure of TPE−mPEG was confirmed by ^{1}H nuclear magnetic resonance (NMR; Supporting Information Figure S1), and the molecular weight of TPE−mPEG was confirmed by matrix assisted laser desoprtion/ionization time-of-flight mass spectroscopy (MALDI-TOF-MS). MALDI-TOF-MS analysis showed that the molecular weight of $mPEG_{2000}$−NH_2 was right-shifted after conjugation, indicating that TPE was successfully grafted (Figure 2C). The purity of TPE−mPEG, confirmed by HPLC, was about 95% (Figure 2D). Since TPE−mPEG possessed an amphiphilic structure, it could self-assemble into micelles (TPEM) in aqueous solution with critical micelle formation concentrations of 6.38 μg/mL (Figure 2E). Contrasting with traditional fluorescence dyes, such as FITC, the fluorescence intensity of these TPE-based micelles was more stable and much less susceptible to laser quenching for up to 1 h (Supporting Information Figure S2). Therefore, we used TPEM to encapsulate doxorubicin (DOX), a typical hydrophobic anticancer drug which can be used for tracing drug delivery and cancer treatment. TPEM micelles loaded with DOX (TPED) were prepared by the film dispersion method. After filtration to remove the free DOX, HPLC was used to characterize the homogeneity of the DOX-loaded micelles. The overlapping elution profiles of TPED monitored at 284 and 477 nm, to detect absorbance from TPE and DOX, respectively, verified that DOX was encapsulated in the micelles (Figure 2F). The morphologies of TPEM and TPED were determined by transmission electron microscopy (TEM) (Figure 3A and B), and the size distributions were measured by dynamic laser light scattering (DLS) (Supporting Information Figure S3). Both TPEM and TPED were spherical in shape, with a diameter of about 30 nm, and had good dispersion. Furthermore, TPED had high encapsulation efficiency (98.4% by weight) and high drug-loading capacity (15.3% by weight).

Spatial Distributions of AIE Micelles in Vitro. We examined whether these AIE micelles were self-traceable in cancer cells during drug delivery. We first tested the fluorescence (FL) intensity of TPE−mPEG in water (non-benign solvent) and methyl alcohol (benign solvent) under the same intensity of ultraviolet absorption and found that the FL intensity of mono-dispersed TPE−mPEG in methyl alcohol was negligible compared to the high emission of the micelles in water (Supporting Informatino Figure S4). On the basis of this observation, the fluorescence spectra of TPEM, TPED, and free DOX were measured to ensure that both TPE and DOX could be excited after DOX was encapsulated in the micelles. As shown in Figure 3C and D, we found that the fluorescence of DOX and TPE could be excited at 330 nm, although the fluorescence intensity of both TPE and DOX decreased upon forming TPED compared to the same concentration of TPEM and free DOX. We hypothesized that this phenomenon was due to fluorescence resonance energy transfer (FRET) because of the overlap between the emission of TPE and the absorption of DOX (Supporting Information Figure S5), but the ACQ effect of DOX in TPED partially reduced the fluorescence intensity efficiency of FRET. Even so, the results still confirmed

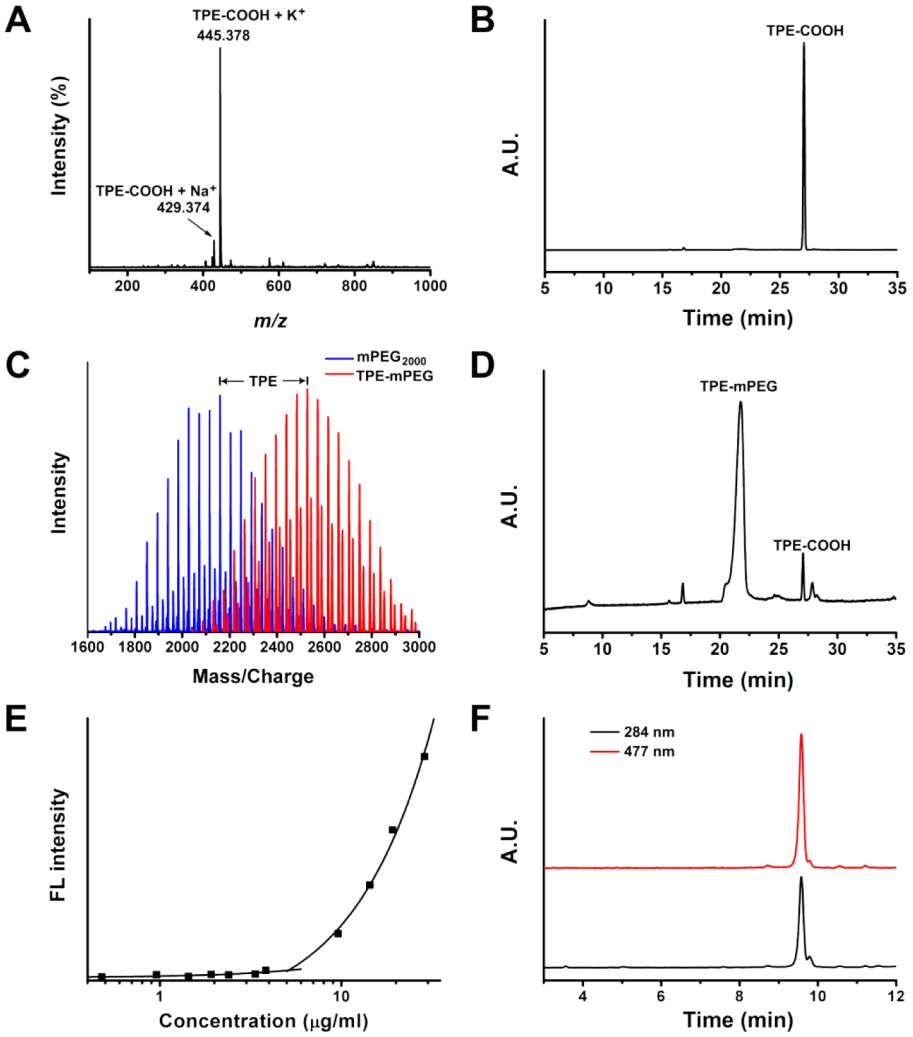

Figure 2. Structural characterization of TPE−COOH, TPE−mPEG, TPE-based micelles (TPEM), and DOX-loaded micelles (TPED). (A) Characterization of TPE−COOH by ESI-MS. (B) HPLC trace of TPE−COOH monitored at 330 nm. (C) MALDI-TOF-MS analysis of the conjugation of TPE−COOH with mPEG−NH_2. (D) HPLC trace of TPE−mPEG monitored at 330 nm. (E) Determination of the critical micelle formation concentration (CMC) of TPE−mPEG and the fluorescence intensity of TPE as a function of the concentration of TPE−mPEG. (F) HPLC traces of DOX-loaded micelles (TPED) monitored at 284 nm (TPE) and 477 nm (DOX), showing a relatively homogeneous morphology with aggregation.

that fluorescence of both TPE and DOX could be excited upon the formation of TPED nanocapsules. Furthermore, the intactness of TPED was examined in the presence of serum by monitoring the change of TPE and DOX FL intensity. If TPED disassembled, the FL intensity of TPE would decrease or disappear. Alternatively, if DOX leaked out of TPED, the fluorescence of the DOX would increase because it is no longer quenched by ACQ efffect and the fluorescence of the TPE would increase because the emission from TPE is no longer transferred by FRET to DOX. As shown in Supporting Information Figure S6, after 24 h incubation with serum, the FL intensity of TPE showed almost no change, which illustrated that TPED was intact in serum. The FL intensity of DOX was slightly enhanced after incubating with serum for 24 h. We supposed that this might be due to the leakage of a small percentage of DOX from TPED.

Next, TPEM and TPED were incubated in vitro with MCF-7 human breast cancer cells for 0.5 and 4 h to observe their intercellular locations by confocal laser scanning microscopy (CLSM) (Figure 4). As shown in CLSM images of TPEM and TPED groups, the fluorescence of TPE ("blue" color) was clearly visible in the cytoplasm, but not in the nucleus, which indicated that TPE−mPEG molecules did not enter into the nucleus. In CLSM images of TPED groups, the blue fluorescence of TPE was colocalized with the fluorescence of DOX ("red" color) in the cytoplasm (giving a "purple" color), suggesting that some of the DOX was still encapsulated in the micelles. After incubating cancer cells with TPED for 4 h, the red fluorescence of DOX was mostly visible in the nucleus, which indicated that our nanocapsules could release DOX into the nucleus. In addition, as the incubation time increased from 0.5 to 4 h, the fluorescence intensity of both DOX and TPE increased, indicating increased cellular uptake of TPEM and TPED.

Localization and Endocytosis Pathway of AIE Micelles In Vitro. In CLSM images of TPED treatment (Figure 4), each cell showed a region with particularly high purple fluorescence intensity near the nucleus (indicated by the white arrows). We hypothesized that these regions corresponded to lysosomes, where TPED was located. As the localization of TPED in the

dx.doi.org/10.1021/am5005267 | ACS Appl. Mater. Interfaces 2014, 6, 5212−5220

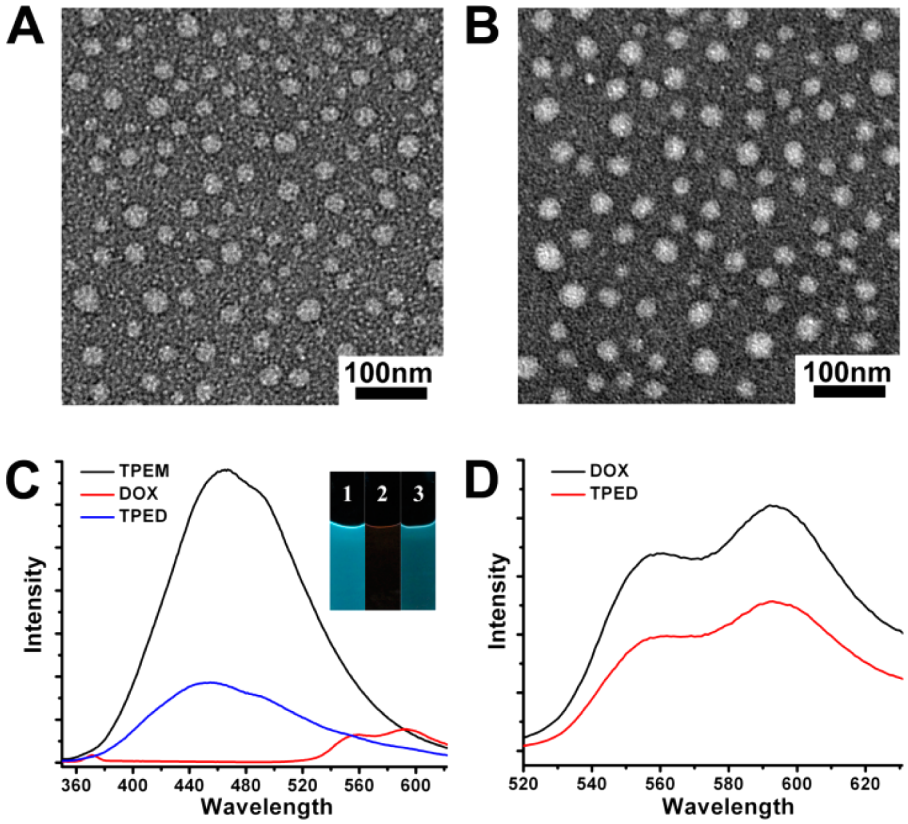

Figure 3. Characterization of TPE-based micelles (TPEM) and DOX-loaded micelles (TPED). (A) TEM image of TPEM after staining with 1% uranyl acetate. (B) TEM image of TPED after staining with 1% uranyl acetate. (C) Fluorescence spectra of TPEM, free DOX, and TPED excited at 330 nm. (inset) Photograph showing fluorescence of TPEM (1), DOX (2), and TPED (3) under UV light (365 nm). (D) Fluorescence spectra of free DOX and TPED excited at 477 nm.

cytoplasm was relevant to the uptake pathway, we investigated the internalization of TPED in MCF-7 cells (Supporting Information Figure S7). Active uptake is significantly reduced at low temperature (4 °C), and we found that the amount of TPED internalized by cells treated at 4 °C was only 19.85% of that of the control group. The ATP synthesis inhibitors sodium azide and 2-deoxy-D-glucose (DOG) reduced the uptake of TPED to 80.67%. The difference between the two inhibition treatments may be due to their different inhibition efficiency. Thus, we came to the conclusion that the pathway by which TPED was taken up into MCF-7 cells was energy-dependent endocytosis. There are two main mechanisms of endocytosis in non-phagocytic cells, clathrin-mediated and lipid raft-mediated. We selected two different inhibitors for each pathway to determine which one was responsible for the uptake of TPED. The results showed that sucrose and chlorpromazine, both of which are clathrin-mediated endocytosis inhibitors, reduced the uptake of TPED, while two inhibitors of lipid raft -mediated endocytosis, nystatin and methyl-β-cyclodextrin (MβCD), did not affect the uptake. This suggests that lipid raft-mediated endocytosis was not involved in the uptake of TPED, and TPED was internalized by MCF-7 cells through clathrin-mediated endocytosis. TPED would then be delivered to lysosomes after they entered into cancer cells.

In order to further investigate the colocalization of TPED and lysosomes, staining of lysosomes with LysoTracker Green DND-26 was performed. As shown in Figure 5, the blue fluorescence of TPE from TPEM and TPED treatments mostly colocalized with the "green" fluorescence of lysotracker near the nucleus. For cells treated with TPED, the areas of co-localization correspond to the purple regions indicated by arrows in TPED-treated cells in Figure 4. Thus, by tracing DOX delivery, we concluded that the nanovehicles were distributed in the cytoplasm and did not enter the nucleus, while DOX could be detached from the nanovehicles and enter the nucleus. In addition, the results also hinted at a plausible DOX release process. Free DOX is very hydrophobic, and so, it tends to be encapsulated in the hydrophobic part of TPEM. Upon entering into cancer cells, TPED experiences a gradually acidified environment inside the lysosomes, and the proto-nation of DOX causes electrostatic repulsion between the drug molecules. Meanwhile, DOX becomes more hydrophilic and the hydrophobic interaction between drug molecules and TPE molecules decreases, so the protonated drug molecules tend to be released from the vehicles and enter into the nucleus[40,41] while TPE−mPEG remains assembled in the cytoplasm as light-emitting micelles.

In Vitro Drug Release and Delivery. To further investigate the drug delivery capability, the release of DOX from TPED nanocapsules in vitro was determined (Figure 6). Because the pH in lysosomes is lower than the cytoplasm,[42,43] the DOX release profile was evaluated by dialysis method at pH 7.4 and 5.0. As shown in Figure 6A, drug release from TPED was much higher at pH 5.0 (85%) than at pH 7.4 (27%). Furthermore, to examine the intracellular uptake and drug release abilities, flow cytometry was used to measure the ability of TPED to enter cancer cells. Human breast cancer MCF-7 cells were incubated with TPED containing 7.5 μM DOX for

dx.doi.org/10.1021/am5005267 | ACS Appl. Mater. Interfaces 2014, 6, 5212−5220

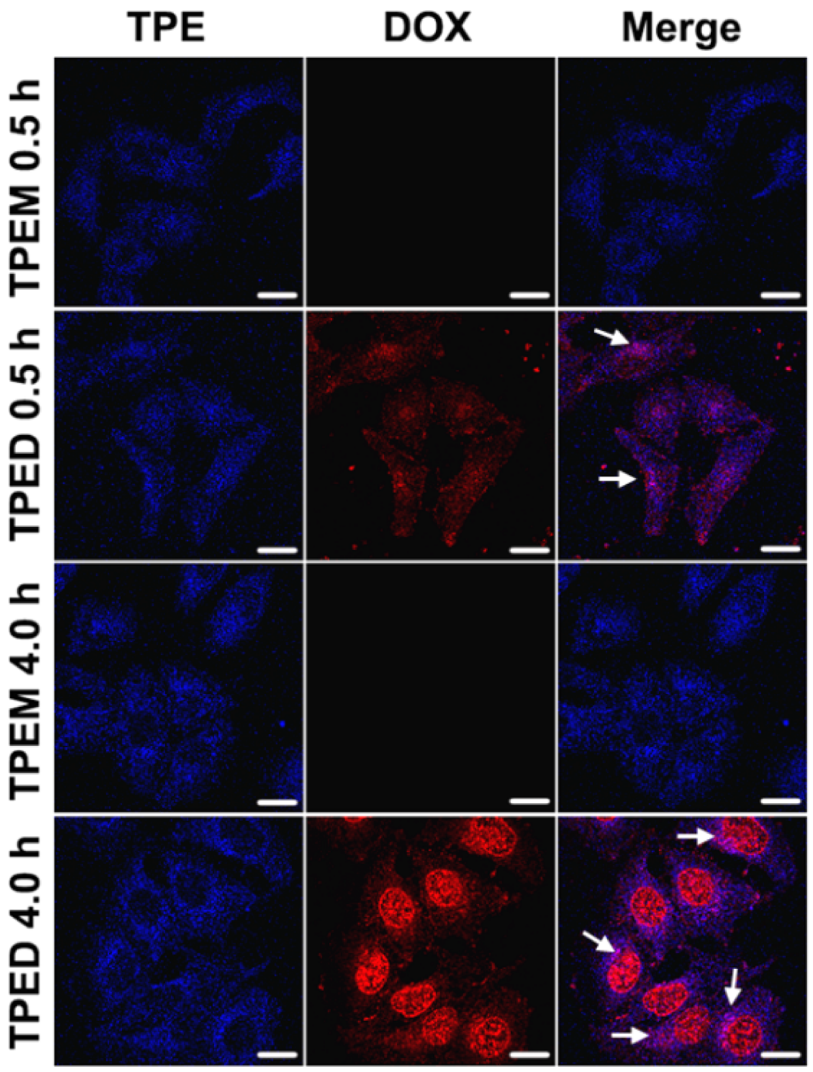

Figure 4. Spatial distributions of TPEM and TPED in MCF-7 cells. CLSM images of the distribution of self-indicating TPEM and TPED. MCF-7 breast cancer cells were incubated with TPEM (75 μM) and TPED (TPE−mPEG 75 μM and DOX 5.0 μM) for 0.5 and 4 h. Scale bars are 20 μm.

0.5 and 4 h with free DOX as a control. As shown in Figure 6B and C, we made quantitative measurements of the cellular uptake of free DOX and TPED. Compared to free DOX, MCF-7 cells treated with TPED after 4 h showed a right shift, suggesting greater cellular uptake of the DOX-loaded nanocapsules. In addition, cellular uptake increased as the incubation time increased from 0.5 to 4 h. Almost all cells were able to internalize free DOX and TPED, since nearly 100% of cells had increased fluorescence except the control group (Figure 6D).

Cytotoxicity Studies of AIE Micelles. Once it was confirmed that TPED could deliver DOX into the nucleus, the overall cytotoxicity of TPED was evaluated and compared with free DOX using the MTT assay. The empty TPEM nanocapsules, with no loaded DOX, were also evaluated under identical conditions. After incubating cells with free DOX or TPED with equal DOX concentrations (0.1−10 μM) for 24 and 48 h, we found that TPED was more toxic to MCF-7 cancer cells (Figure 7A and B). As depicted in Figure 7, TPED showed a lower IC_{50} (about 1.2 μM) than free DOX (about 3.0 μM). In addition, the results also indicated that TPEM had little toxicity to MCF-7 cells at concentrations corresponding to the amount of micelles used in the TPED treatment. Even when the concentration increased to 100 μM, no clear toxicity was observed (Supporting Information Figure S8). Hence, the lower IC_{50} of TPED was not due to the toxic effect of TPE−mPEG molecules but, rather, was caused by the enhanced cellular internalization of DOX when encapsulated into micelles.

■ CONCLUSION

Herein, we demonstrated a novel concept of directly using TPE to create nanocarriers that display AIE for tracing intracellular anticancer drug delivery. When loaded with DOX, TPE−mPEG formed a stable micelle, and this hydrophobic drug delivery system showed higher antitumor efficiency than free DOX in vitro, while TPE−mPEG itself displayed no cytotoxicity. The micelles can be employed for intracellular imaging and self-localization due to the AIE property. This study thus opens up new approaches to the design of traceable drug delivery systems.

■ EXPERIMENTAL SECTION

Materials and Reagents. Amino-methoxypolyethylene glycol ($mPEG_{2000}$−NH_2) was purchased from PegBio Co., Ltd (Suzhou, China). *O*-(7-Azabenzotriazole-1-yl)-1,1,3,3-tetramethyluronilum hexafluorophosphate (HATU) and Diisopropylethylamine (DIEA) were

dx.doi.org/10.1021/am5005267 | ACS Appl. Mater. Interfaces 2014, 6, 5212−5220

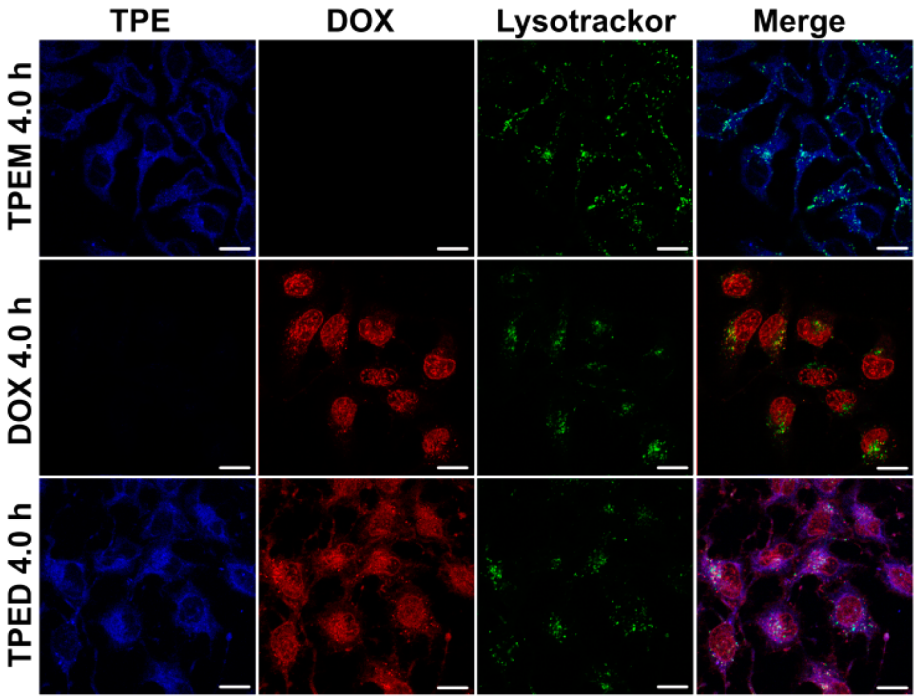

Figure 5. Detailed spatiotemporal distributions of TPEM, DOX, and TPED co-localized with lysosomes in MCF-7 cells. Scale bars are 20 μm.

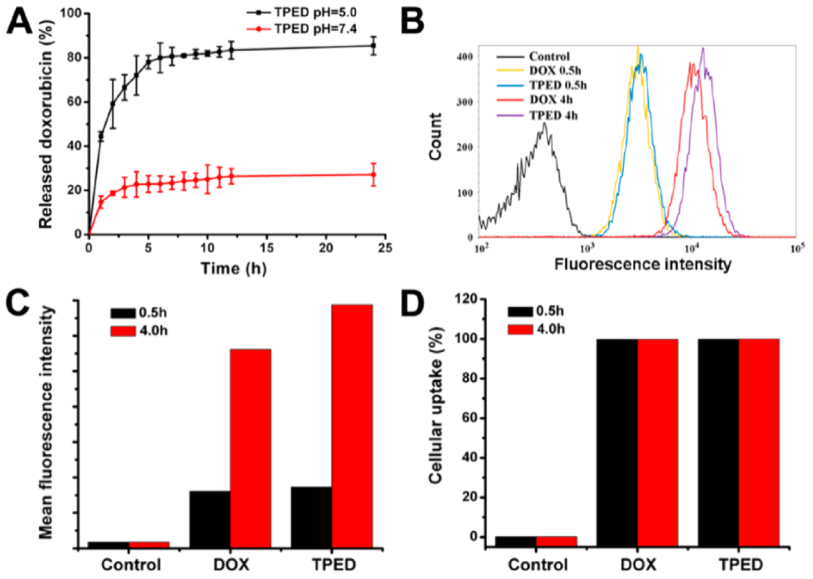

Figure 6. Time course of DOX release from TPED and cellular uptake of free DOX and TPED by MCF-7 cells. (A) Time course of DOX release from TPED at 37 °C at pH 5.0 or 7.4. Released DOX was separated from TPED by dialysis and quantified by spectrophotometer. (B) Quantitative analysis of free DOX and TPED uptake by flow cytometry. (C) Mean fluorescence intensity of cells after 0.5 or 4 h. Control cells were untreated. (D) Percentages of cells with increased fluorescence.

purchased from BO MAI JIE Technology Co., Ltd (Beijing, China). Doxorubicin hydrochloride was obtained from Beijing Huafeng United Technology Co., Ltd (Beijing, China). Other chemical reagents and solvents were obtained from Alfa and used as received.

Dulbecco's modified eagle's medium (DMEM) and fetal bovine serum were obtained from Wisent Inc. (Multicell, Wisent Inc., St. Bruno, Quebec, Canada). Also, 0.25% trypsin−EDTA and antibiotic solution (penicillin and streptomycin) were purchased from Invitrogen (Invitrogen, Carlsbad, CA). The human breast cancer cell line MCF-7 was purchased from American Type Culture Collection (ATCC; Manassas, VA). Culture dishes and plates were from Corning (Corning, New York, USA). MCF-7 cells were maintained in DMEM with 10% fetal bovine serum and 1% antibiotic solution. All cells were cultured in a humidified atmosphere containing 5% CO_2 at 37 °C.

Synthesis of TPE−mPEG. In the synthesis of TPE−mPEG, carboxylated tetraphenylethylene (TPE−COOH) was first synthesized. We first prepared TPE derivative 1 using the McMurry reaction and then treated derivative 1 with BBr_3 and obtained derivative 2 smoothly. Derivative 2 was treated with methyl 2-bromoacetate in the presence of K_2CO_3 and then TPE derivative 3 was obtained. Subsequently, treatment of derivative 3 with LiOH gave TPE−COOH. To synthesize TPE−mPEG, TPE−COOH was dissolved in anhydrous dichloromethane at room temperature. HATU and DIEA were added into this solution and stirred continuously at room teperature for 2 min. When a yellow solution formed, amino-

dx.doi.org/10.1021/am5005267 | ACS Appl. Mater. Interfaces 2014, 6, 5212−5220

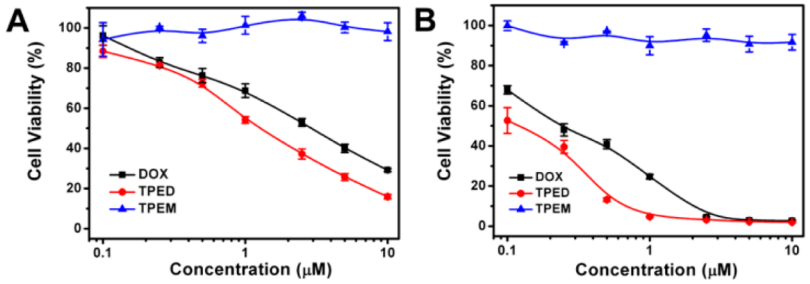

Figure 7. In vitro cytotoxicity of free DOX, TPEM, and TPED to MCF-7 breast cancer cells determined by MTT assay. Cells were treated for 24 (A) and 48 h (B), respectively.

methoxypolyethylene glycol dissolved in dichloromethane was added dropwise into this solution, which was stirred continuously at room temperature for 48 h. The solvent was removed under vacuum. The remaining residue was dissolved in water and then purified by dialysis with a molecular weight cutoff of 3500 Da. The reaction product was lyophilized and analyzed by MALDI-TOF-MS using a Microflex LRF System spectrometer (Bruker Daltonics, USA).

Determination of the Critical Micelle Formation Concentration (CMC) of TPE−mPEG. Owing to the aggregation-induced emission of the TPE moiety, which can self-indicate the formation of micelles, a simple method was established to determine the CMC by detecting the emergence of the fluorescence of TPE when TPE−mPEG was assembled in phosphate buffer. A measured amount of TPE−mPEG solution was added to vials and phosphate buffer of pH 7.4 was added to the vials to obtain TPE−mPEG solutions with concentrations ranging from 0.48 to 28.8 μg/mL. The vials were sonicated for 10 minutes, and then, the fluorescence intensity at a wavelength of 460 nm (excited at 330 nm) was measured using a fluorescence spectrophotometer (HITACHI F-4600). The critical micelle concentration was obtained as the intersection of the tangents to the two linear portions of the graph of the fluorescence intensity as a function of TPE−mPEG concentration.

Preparation of DOX-Loaded Micelles. DOX-loaded micelles (TPED) were prepared from DOX and TPE−mPEG via the film dispersion method. A measured amount of DOX was dissolved in 1 mL methanol at room temperature (molar ratio of DOX:triethylamine = 1:2) and mixed with TPE−mPEG in 2 mL chloroform. The solvent was removed under vacuum rotary evaporation to form a dry film. The dried film was hydrated with phosphate buffer of pH 7.4 for 1 h. Nonencapsulated DOX was separated by filtering the micelle suspension through a 220 nm polycarbonate membrane (Millipore Co., Bedford, MA). To confirm the concentration of DOX in micelles, TPED was dissolved in methanol to destroy the structure of micelles and release free DOX into methanol. The concentration of free DOX in methanol was determined using a Perkin-Elmer LS 55 luminescence spectrometer (Perkin-Elmer Instruments Co., Ltd., USA) with 488 nm excitation and 591 nm emission.

Characterization of Micelles. The morphologies of TPEM and TPED were determined using a Hitachi HT7700 transmission electron microscope (TEM) with 120 kV acceleration voltage. Micelles were prestained with 1% uranyl acetate. Particle size was determined by dynamic light scattering (DLS) using a Zetasizer 5000 (Malvern Instruments, Malvern, Worcestershire, U.K.). The homogeneity of the DOX-loaded micelles was characterized by high-performance liquid chromatography (HPLC; Waters 2796, USA).

Subcellular Localization of Micelles and Imaging. For confocal microscopy, 10^6 MCF-7 cells were seeded into 35 mm microscopy dishes, incubated at 37 °C for 24 h and then incubated with free DOX, TPEM, and TPED (TPE−mPEG 75 μM and DOX 5.0 μM) for 0.5 and 4 h at 37 °C. Cells were imaged using a confocal laser scanning microscopy (LSM710, Carl Zeiss Microscopy) with excitation at 405 nm for TPE and 488 nm for DOX.

Free DOX and TPED Uptake by Breast Cancer Cells. Cellular uptake of free DOX and TPED was investigated by quantitative flow cytometry analysis. For flow cytometry, 3×10^5 cells per well were seeded into 6-well plates, then cultured with free DOX or TPED at the same concentration. Cells were washed with PBS, harvested, and analyzed using an Attune® acoustic focusing cytometer (Applied Biosystems, Life Technologies, Carlsbad, CA).

Cytotoxicity Studies. MCF-7 cells were seeded at 5×10^3 cells per well in a 96-well plate, pre-incubated for 24 h, and then incubated with free DOX or TPED for 24 and 48 h at DOX concentrations ranging from 0.1 to 10 μM. The medium was replaced with 100 μL 0.5 mg/mL MTT and after 3 h the MTT solution was replaced with 150 μL DMSO solution. The absorbance was measured at 570 nm with a reference wavelength of 630 nm using an Infinite M200 microplate reader (Tecan, Durham, USA). Untreated cells in medium were used as the control. The cytotoxicity of empty TPE−mPEG micelles (TPEM) was also tested by using the method above. The concentration of empty micelles ranged from 0.1 to 100 μM.

■ ASSOCIATED CONTENT

Supporting Information

Laser photo bleaching experiment, dynamic light scattering, fluorescent spectra, stability of TPED in serum-supplemented medium, endocytosis inhibition experiment, cytotoxicity studies, and Figures S1−7. This material is available free of charge via the Internet at http://pubs.acs.org.

■ AUTHOR INFORMATION

Corresponding Authors

*Fax: +86-010-62656765. Tel.: +86-010-82545530. E-mail: zougz@nanoctr.cn.

*E-mail: liangxj@nanoctr.cn.

Author Contributions

§C.Z. and S.J.: These authors contributed equally.

Notes

The authors declare no competing financial interest.

■ ACKNOWLEDGMENTS

This work was financially supported in part by grants from the State High-Tech Development Plan (2012AA020804), National Natural Science Foundation of China project (Nos. 30970784, 31170873, and 81171455), National Key Basic Research Program of China (2009CB930200), National Distinguished Young Scholars grant (31225009) from the National Natural Science Foundation of China, and Chinese Academy of Sciences (CAS) "Hundred Talents Program" (07165111ZX).

■ REFERENCES

(1) Lee, C. C.; MacKay, J. A.; Frechet, J. M.; Szoka, F. C. Designing Dendrimers for Biological Applications. *Nat. Biotechnol.* **2005**, *23*, 1517−1526.

(2) Gillies, E. R.; Jonsson, T. B.; Frechet, J. M. Stimuli-Responsive Supramolecular Assemblies of Linear-Dendritic Copolymers. *J. Am. Chem. Soc.* **2004**, *126*, 11936−11943.
(3) Lee, C. C.; Gillies, E. R.; Fox, M. E.; Guillaudeu, S. J.; Frechet, J. M.; Dy, E. E.; Szoka, F. C. A Single Dose of Doxorubicin-Functionalized Bow-Tie Dendrimer Dures Mice Bearing C-26 Colon Carcinomas. *Proc. Natl. Acad. Sci. USA* **2006**, *103*, 16649−16654.
(4) Kolhatkar, R. B.; Swaan, P.; Ghandehari, H. Potential Oral Delivery of 7-Ethyl-10-Hydroxy-Camptothecin (SN-38) Using Poly(amidoamine) Dendrimers. *Pharm. Res.* **2008**, *25*, 1723−1729.
(5) Geng, Y.; Discher, D. E. Hydrolytic Degradation of Poly(ethylene oxide)-Block-Polycaprolactone Worm Micelles. *J. Am. Chem. Soc.* **2005**, *127*, 12780−12781.
(6) Soussan, E.; Cassel, S.; Blanzat, M.; Rico-Lattes, I. Drug Delivery by Soft Matter: Matrix and Vesicular Carriers. *Angew. Chem. Int. Ed.* **2009**, *48*, 274−288.
(7) Sapra, P.; Tyagi, P.; Allen, T. M. Ligand-Targeted Liposomes for Cancer Treatment. *Curr. Drug. Deliv.* **2005**, *2*, 369−381.
(8) Lee, S. M.; Chen, H.; Dettmer, C. M.; O'Halloran, T. V.; Nguyen, S. T. Polymer-Caged Lipsomes: a pH-Responsive Delivery System with High Stability. *J. Am. Chem. Soc.* **2007**, *129*, 15096−15097.
(9) Linderoth, L.; Fristrup, P.; Hansen, M.; Melander, F.; Madsen, R.; Andresen, T. L.; Peters, G. H. Mechanistic Study of the sPLA2-Mediated Hydrolysis of a Thio-Ester Pro Anticancer Ether Lipid. *J. Am. Chem. Soc.* **2009**, *131*, 12193−12200.
(10) Weng, K. C.; Noble, C. O.; Papahadjopoulos-Sternberg, B.; Chen, F. F.; Drummond, D. C.; Kirpotin, D. B.; Wang, D.; Hom, Y. K.; Hann, B.; Park, J. W. Targeted Tumor Cell Internalization and Imaging of Multifunctional Quantum Dot-Conjugated Immunoliposomes in vitro and in vivo. *Nano Lett.* **2008**, *8*, 2851−2857.
(11) Volodkin, D. V.; Skirtach, A. G.; Mohwald, H. Near-IR Remote Release from Assemblies of Liposomes and Nanoparticles. *Angew. Chem. Int. Ed.* **2009**, *48*, 1807−1809.
(12) Linderoth, L.; Peters, G. H.; Madsen, R.; Andresen, T. L. Drug Delivery by an Enzyme-Mediated Cyclization of a Lipid Prodrug with Unique Bilayer-Formation Properties. *Angew. Chem. Int. Ed.* **2009**, *48*, 1823−1826.
(13) Wu, G.; Mikhailovsky, A.; Khant, H. A.; Fu, C.; Chiu, W.; Zasadzinski, J. A. Remotely Triggered Liposome Release by Near-Infrared Light Absorption via Hollow Gold Nanoshells. *J. Am. Chem. Soc.* **2008**, *130*, 8175−8177.
(14) Chen, J.; Ouyang, J.; Kong, J.; Zhong, W.; Xing, M. M. Photo-Cross-Linked and pH-Sensitive Biodegradable Micelles for Doxorubicin Delivery. *ACS Appl. Mater. Interfaces.* **2013**, *5*, 3108−3117.
(15) Nasongkla, N.; Bey, E.; Ren, J.; Ai, H.; Khemtong, C.; Guthi, J. S.; Chin, S. F.; Sherry, A. D.; Boothman, D. A.; Gao, J. Multifunctional Polymeric Micelles as Cancer-Targeted, MRI-Ultrasensitive Drug Delivery Systems. *Nano Lett.* **2006**, *6*, 2427−2430.
(16) Luo, J.; Xiao, K.; Li, Y.; Lee, J. S.; Shi, L.; Tan, Y. H.; Xing, L.; Holland Cheng, R.; Liu, G. Y.; Lam, K. S. Well-Defined, Size-Tunable, Multifunctional Micelles for Efficient Paclitaxel Delivery for Cancer Treatment. *Bioconjug. Chem.* **2010**, *21*, 1216−1224.
(17) Koizumi, F.; Kitagawa, M.; Negishi, T.; Onda, T.; Matsumoto, S.; Hamaguchi, T.; Matsumura, Y. Novel SN-38-Incorporating Polymeric Micelles, NK012, Eradicate Vascular Endothelial Growth Factor-Secreting Bulky Tumors. *Cancer Res.* **2006**, *66*, 10048−10056.
(18) Kam, N. W.; Liu, Z.; Dai, H.; Chen, L.; Li, L.; Zhang, L.; Xing, S.; Wang, T.; Wang, Y. A.; Wang, C.; Su, Z. Designed Fabrication of Unique Eccentric Mesoporous Silica Nanocluster-Based Core-Shell Nanostructures for pH-Responsive Drug Delivery. *ACS Appl. Mater. Interfaces.* **2013**, *5*, 7282−7290.
(19) Prencipe, G.; Tabakman, S. M.; Welsher, K.; Liu, Z.; Goodwin, A. P.; Zhang, L.; Henry, J.; Dai, H. PEG Branched Polymer for Functionalization of Nanomaterials with Ultralong Blood Circulation. *J. Am. Chem. Soc.* **2009**, *131*, 4783−4787.
(20) Huo, Q.; Liu, J.; Wang, L. Q.; Jiang, Y.; Lambert, T. N.; Fang, E. A New Class of Silica Cross-Linked Micellar Core-Shell Nanoparticles. *J. Am. Chem. Soc.* **2006**, *128*, 6447−6453.
(21) Horcajada, P.; Serre, C.; Maurin, G.; Ramsahye, N. A.; Balas, F.; Vallet-Regi, M.; Sebban, M.; Taulelle, F.; Ferey, G. Flexible Porous Metal-Organic Frameworks for a Controlled Drug Delivery. *J. Am. Chem. Soc.* **2008**, *130*, 6774−6780.
(22) Chen, J.; Chen, S.; Zhao, X.; Kuznetsova, L. V.; Wong, S. S.; Ojima, I. Functionalized Single-Walled Carbon Nanotubes as Rationally Designed Vehicles for Tumor-Targeted Drug Delivery. *J. Am. Chem. Soc.* **2008**, *130*, 16778−16785.
(23) Cheng, Y.; A, C. S.; Meyers, J. D.; Panagopoulos, I.; Fei, B.; Burda, C. Highly Efficient Drug Delivery with Gold Nanoparticle Vectors for in vivo Photodynamic Therapy of Cancer. *J. Am. Chem. Soc.* **2008**, *130*, 10643−10647.
(24) Liu, Z.; Robinson, J. T.; Sun, X.; Dai, H. PEGylated Nanographene Oxide for Delivery of Water-Insoluble Cancer Drugs. *J. Am. Chem. Soc.* **2008**, *130*, 10876−10877.
(25) Maeda, H.; Nakamura, H.; Fang, J. The EPR Effect for Macromolecular Drug Delivery to Solid Tumors: Improvement of Tumor Uptake, Lowering of Systemic Toxicity, and Distinct Tumor Imaging in vivo. *Adv. Drug. Deliv. Rev.* **2013**, *65*, 71−79.
(26) Peer, D.; Karp, J. M.; Hong, S.; Farokhzad, O. C.; Margalit, R.; Langer, R. Nanocarriers as an Emerging Platform for Cancer Therapy. *Nat. Nanotechnol.* **2007**, *2*, 751−760.
(27) Lee, S. J.; Park, K.; Oh, Y. K.; Kwon, S. H.; Her, S.; Kim, I. S.; Choi, K.; Lee, S. J.; Kim, H.; Lee, S. G.; Kim, K.; Kwon, I. C. Tumor Specificity and Therapeutic Efficacy of Photosensitizer-Encapsulated Glycol Chitosan-Based Nanoparticles in Tumor-Bearing Mice. *Biomaterials* **2009**, *30*, 2929−2939.
(28) Lee, S. J.; Koo, H.; Jeong, H.; Huh, M. S.; Choi, Y.; Jeong, S. Y.; Byun, Y.; Choi, K.; Kim, K.; Kwon, I. C. Comparative Study of Photosensitizer Loaded and Conjugated Glycol Chitosan Nanoparticles for Cancer Therapy. *J. Control. Release* **2011**, *152*, 21−29.
(29) Cui, S.; Yin, D.; Chen, Y.; Di, Y.; Chen, H.; Ma, Y.; Achilefu, S.; Gu, Y. In vivo Targeted Deep-Tissue Photodynamic Therapy On the basis of Near-Infrared Light Triggered Upconversion Nanoconstruct. *ACS Nano* **2013**, *7*, 676−688.
(30) Choi, K. Y.; Liu, G.; Lee, S.; Chen, X. Theranostic Nanoplatforms for Simultaneous Cancer Imaging and Therapy: Current Approaches and Future Perspectives. *Nanoscale* **2012**, *4*, 330−342.
(31) Chen, C.; Geng, J.; Pu, F.; Yang, X.; Ren, J.; Qu, X. Polyvalent Nucleic Acid/Mesoporous Silica Nanoparticle Conjugates: Dual Stimuli-Responsive Vehicles for Intracellular Drug Delivery. *Angew. Chem. Int. Ed.* **2011**, *50*, 882−886.
(32) Liong, M.; Lu, J.; Kovochich, M.; Xia, T.; Ruehm, S. G.; Nel, A. E.; Tamanoi, F.; Zink, J. I. Multifunctional Inorganic Nanoparticles for Imaging, Targeting, and Drug Delivery. *ACS Nano* **2008**, *2*, 889−896.
(33) Chen, J. I.; Wu, W. C. Fluorescent Polymeric Micelles with Aggregation-Induced Emission Properties for Monitoring the Encapsulation of Doxorubicin. *Macromol. Biosci.* **2013**, *13*, 623−632.
(34) Xue, X.; Zhao, Y.; Dai, L.; Zhang, X.; Hao, X.; Zhang, C.; Huo, S.; Liu, J.; Liu, C.; Kumar, A.; Chen, W. Q.; Zou, G.; Liang, X. J. Spatiotemporal Drug Release Visualized through a Drug Delivery System with Tunable Aggregation-Induced Emission. *Adv. Mater.* **2014**, *26*, 712−717.
(35) Yuan, Y.; Kwok, R. T.; Tang, B. Z.; Liu, B. Targeted Theranostic Platinum(IV) Prodrug with a Built-In Aggregation-Induced Emission Light-Up Apoptosis Sensor for Noninvasive Early Evaluation of Its Therapeutic Responses in Situ. *J. Am. Chem. Soc.* **2014**, *136*, 2546−2554.
(36) Zhao, Z.; Lam, J. W. Y.; Tang, B. Z. Tetraphenylethene: a Versatile AIE Building Block for the Construction of Efficient Luminescent Materials for Organic Light-Emitting Diodes. *J. Mater. Chem.* **2012**, *22*, 23726−23740.
(37) Huang, X.; Gu, X.; Zhang, G.; Zhang, D. A Highly Selective Fluorescence Turn-on Detection of Cyanide Based on the Aggregation of Tetraphenylethylene Molecules Induced by Chemical Reaction. *Chem. Commun.* **2012**, *48*, 12195−12197.
(38) Xu, X.; Li, J.; Li, Q.; Huang, J.; Dong, Y.; Hong, Y.; Yan, J.; Qin, J.; Li, Z.; Tang, B. Z. A Strategy for Dramatically Enhancing the

Selectivity of Molecules Showing Aggregation-Induced Emission towards Biomacromolecules with the Aid of Graphene Oxide. *Chemistry* **2012**, *18*, 7278−7286.
(39) Zhao, Z.; Lam, J. W.; Chan, C. Y.; Chen, S.; Liu, J.; Lu, P.; Rodriguez, M.; Maldonado, J. L.; Ramos-Ortiz, G.; Sung, H. H.; Williams, I. D.; Su, H.; Wong, K. S.; Ma, Y.; Kwok, H. S.; Qiu, H.; Tang, B. Z. Stereoselective Synthesis, Efficient Light Emission, and High Bipolar Charge Mobility of Chiasmatic Luminogens. *Adv. Mater.* **2011**, *23*, 5430−5435.
(40) Mohan, P.; Rapoport, N. Doxorubicin as a Molecular Nanotheranostic Agent: Effect of Doxorubicin Encapsulation in Micelles or Nanoemulsions on the Ultrasound-Mediated Intracellular Delivery and Nuclear Trafficking. *Mol. Pharmaceutics* **2010**, *7*, 1959−1973.
(41) Wei, T.; Liu, J.; Ma, H.; Cheng, Q.; Huang, Y.; Zhao, J.; Huo, S.; Xue, X.; Liang, Z.; Liang, X. J. Functionalized Nanoscale Micelles Improve Drug Delivery for Cancer Therapy in Vitro and in Vivo. *Nano Lett.* **2013**, *13*, 2528−2534.
(42) Yuan, Q.; Yeudall, W. A.; Yang, H. PEGylated Polyamidoamine Dendrimers with Bis-Aryl Hydrazone Linkages for Enhanced Gene Delivery. *Biomacromolecules* **2010**, *11*, 1940−1947.
(43) Aryal, S.; Hu, C. M.; Zhang, L. Polymer-Displatin Conjugate Nanoparticles for Acid-Responsive Drug Delivery. *ACS Nano* **2010**, *4*, 251−258.